Research on Engineering Structures & Materials
www.jresm.org
Research Group

Research Article

Numerical modeling of the effects of volume fraction and fiber orientation on the elastic modulus of a CNT/polymer-based nanocomposite material

Charafeddine Benatmane *,1,2,a, Samir Brek 1,2,b, Lahcene Ghouari 3,4,c

[1]*Mechanical Engineering Department, Abbes Laghrour University, Khenchela, Algeria*
[2]*Laboratory of Engineering and Sciences of Advanced Materials (ISMA), Abbes Laghrour University, Khenchela, Algeria*
[3]*Mechanical Engineering Department, Dr Yahia Fares of Medea University, Medea, Algeria*
[4]*Laboratory of mathematical, Mechanical and Physical Modeling (LMP2M), University of Medea, Algeria*

Article Info

Article History:

Received 06 Jan 2026

Accepted 14 Aug 2026

Keywords:

Nanocomposite;
Carbon nanotubes;
Polymer;
Elastic modulus;
Finite element method

Abstract

The objective of this study is to predict the elastic modulus (E_c) of polymer/carbon nanotube (CNT) nanocomposites and to analyze the influence of CNT orientation and volume fraction on their mechanical behavior. A finite element numerical model was developed by considering different CNT orientations (horizontal, inclined, vertical, and random), with volume fractions ranging from 1.39% to 5.58%. The numerical results were compared with analytical micromechanical models commonly applied to short fiber reinforced composites. The findings demonstrate that both CNT orientation and volume fraction have a significant influence on the elastic modulus of the nanocomposite. Increasing the CNT volume fraction leads to a progressive enhancement of the Ec. Horizontally aligned CNTs exhibit the highest elastic modulus (E_c=4799.14 MPa), followed by randomly oriented, inclined, and vertically oriented CNT configurations. The predictions obtained using the finite element method show good agreement with the Halpin-Tsai analytical model. For the horizontal CNT configuration, the results are also consistent with the Cox and Lavngood-Goettler models for certain volume fractions. These results highlight the critical role of CNT orientation and content in enhancing the mechanical properties of polymer/CNT nanocomposites and contribute to the optimization of modeling approaches and material design strategies for these advanced materials.

1. Introduction

In recent years, polymer nanocomposites reinforced with carbon nanotubes (CNTs) have attracted considerable attention in the fields of polymer science and engineering because of their outstanding mechanical and physical properties, including high strength, enhanced stiffness, low density, and excellent thermal and electrical conductivity [1-4]. These remarkable characteristics make CNT/polymer nanocomposites promising materials for advanced structural applications requiring improved mechanical performance and lightweight design.

The accurate prediction and characterization of the mechanical behavior of nanocomposites remain challenging. Although experimental approaches provide valuable information, they are often associated with high costs, complex preparation procedures, and time-consuming testing processes [5]. Therefore, numerical and analytical approaches have become essential tools for

*Corresponding author: benatmane.charafeddine@univ-khenchela.dz
[a]orcid.org/0009-0007-2837-8792; [b]orcid.org/0000-0001-7292-5393; [c]orcid.org/ 0009-0009-9776-988X
DOI: http://dx.doi.org/10.17515/resm2026-1454ma0106rs

predicting and optimizing the effective properties of composite materials [6-12]. Among these approaches, representative volume element (RVE) based modeling combined with continuum mechanics has been widely adopted to investigate the influence of nanoscale reinforcement parameters on the macroscopic behavior of nanocomposites [13-15]. Recent advances in the modeling of nanostructured and microstructure materials have highlighted the importance of appropriate theoretical frameworks for accurately describing their mechanical behavior. In particular, several studies have emphasized the necessity of considering size-dependent effects and advanced elasticity theories to capture the physical response of materials at small scales. These developments provide valuable insights into the influence of material architecture, scale effects, and reinforcement mechanisms on the effective properties of advanced composite systems [16, 17].

Several researchers have investigated the mechanical behavior of CNT-reinforced polymer nanocomposites using numerical and analytical approaches. Hassanzadeh-Aghdam et al [18]. evaluated the effective elastic properties of polymer nanocomposites containing regular and randomly distributed CNTs using finite element analysis based on representative volume element (RVE) modeling. Kassa and Arumugam [19]. proposed a numerical methodology supported by experimental validation to predict the elastic properties of CNT-reinforced polymer nanocomposites. Zaccardi et al [20]. developed a multiscale modeling approach to evaluate the mechanical properties of epoxy reinforced with single-walled carbon nanotubes (SWCNTs). Chwał and Muc [21]. analyzed the effects of CNT arrangement patterns, including square and hexagonal distributions, on the elastic properties of CNT/epoxy nanocomposites using finite element modeling. Omari et al [22]. examined the effects of particle size ratio and reinforcement orientation on the elastic modulus of polymer matrices. Imani Yengejeh et al [23]. reviewed experimental and modeling approaches for CNT-reinforced composites, emphasizing the influence of CNT geometry, size, and orientation on their elastic behavior. Moradi et al [24]. developed a finite element-based micromechanical model to investigate the effects of CNT dispersion and agglomeration on the elastic, thermoelastic, and viscoelastic properties of polymer nanocomposites, demonstrating that CNT distribution strongly affects the overall composite performance.

Despite these significant contributions, the combined influence of CNT orientation and volume fraction on the elastic modulus of polymer/CNT nanocomposites remains insufficiently explored. In particular, a systematic investigation of different CNT orientations within a finite element representative volume element (RVE) framework is still needed to better understand their effect on stress transfer mechanisms and the overall mechanical response of nanocomposites. The results of this study provide valuable insights into the design and optimization of CNT/polymer nanocomposites by clarifying the relationship between CNT orientation, volume fraction, and elastic performance. Furthermore, the proposed finite element-based numerical framework provides an efficient predictive tool for optimizing CNT alignment and designing lightweight, high-performance polymer nanocomposites for advanced engineering applications.

This study aims to predict the elastic modulus of a CNT/polymer nanocomposite material and to investigate the influence of CNT volume fraction and orientation on the elastic modulus (E_c) using numerical modeling. Carbon nanotubes were considered as reinforcement, and multiple representative volume elements (RVEs) were constructed to represent different CNT orientations (horizontal, vertical, inclined, and random) and various volume fractions. Finite element numerical simulations were performed using Cast3M software [25,26]. Finally, the numerical results obtained from the RVE-based simulations were compared with analytical micromechanical models to evaluate the accuracy and reliability of the proposed approach.

2. Analytical Models for Short Fiber Composites

2.1 Voigt (1889) and Reuss (1929) Models

The Voigt and Reuss models are the simplest micromechanical models based on the rule of mixtures. The Voigt model assumes that each constituent undergoes the same deformation (iso-deformation condition), leading to an expression for the elastic modulus (E_c), as given in Eq (1) [27, 28].

$$E_c = E_{fl}.V_f + E_m.V_m \tag{1}$$

Where; E_{fl}, V_f respectively denote the characteristics of the fibers (longitudinal elastic modulus and volume fraction), E_m and V_m respectively represent the properties of the matrix (elastic modulus and volume fraction). The Reuss model provides an expression for the elastic modulus (E_c), as given in Eq (2) [27,28], assuming that all phases are subjected to the same stress (iso-stress condition).

$$E_c = \frac{E_{ft}.E_m}{E_m.V_f + E_{ft}.V_m} \tag{2}$$

Where; E_{ft}: transverse fiber elastic modulus.

2.2 Hori and Onogi Model (1951)

Hori and Onogi proposed the following equation for the elastic modulus (E_c), as given in Eq (3) [29, 30].

$$E_c = (E_1.E_2)^{1/2} \tag{3}$$

where the variables E_1 and E_2 are specified according to the Voigt model Eq (1) and the Reuss model Eq (2).

2.3 Cox Model (1952)

The Cox elastic stress transfer model represents a classical approach for analyzing short fiber-reinforced composites. It assumes that both the fibers and the matrix behave elastically, while the fiber-matrix interface efficiently transfers stress without yielding or interfacial slippage, as given in Eq (4) [31,32].

$$E_1 = E_{fl}V_f\eta_l + V_mE_m \tag{4}$$

The parameters used in Eq (4) are calculated based on the formulations proposed by Cox , as given in Eqs. (5-7) [31].

$$\eta_l = 1 - \frac{tanh\,(\frac{\beta l}{2})}{\frac{\beta l}{2}} \tag{5}$$

$$\beta^2 = \frac{2G_m}{E_{1f}r^2 ln\,(\frac{r_0}{r})} \tag{6}$$

$$r_0 = \frac{r}{\sqrt{V_f}} \tag{7}$$

Where η_l is the fiber length efficiency factor, β is the shear-lag parameter, l is the fiber length, G_m is the matrix shear modulus, E_{fl} is the longitudinal modulus of the fiber, r is the fiber radius, r_0 is the effective matrix radius, V_f is the fiber volume fraction, V_m is the matrix volume fraction, and E_m is the matrix Young's modulus [31].

2.4 Halpin-Tsai Model (1968)

The Halpin-Tsai semi-empirical model provides an analytical framework for estimating the Young's modulus of short fiber-reinforced composites, whether the fibers are aligned or randomly distributed. When the fiber volume fraction (V_f) remains low compared with the overall composite volume, the Halpin–Tsai equation takes the following form, as given in Eq (8) [33 -37].

$$E_c = E_m\left[\frac{3}{8}\left(\frac{1+\zeta\eta_L V_f}{1-\eta_L V_f}\right) + \frac{5}{8}\left(\frac{1+2\eta_T V_f}{1-\eta_T V_f}\right)\right] \tag{8}$$

where E_m is the Young's modulus of the matrix, E_f is the Young's modulus of the fiber, V_f is the fiber volume fraction, η_L and η_T are the longitudinal and transverse reinforcement factors, respectively, and ζ is the fiber geometry parameter related to the fiber aspect ratio, which is defined as:

$$\zeta = 2\frac{l}{d} \tag{9}$$

Where (l) is the fiber length and (d) is the fiber diameter.

The longitudinal and transverse reinforcement factors are calculated as follows:

$$\eta_L = \frac{\frac{E_f}{E_m} - 1}{\frac{E_f}{E_m} + \zeta} \tag{10}$$

$$\eta_T = \frac{\frac{E_f}{E_m} - 1}{\frac{E_f}{E_m} + 2} \tag{11}$$

For the calculation of the reinforcement factors, (E_{fl}) was used in the longitudinal factor (η_L), while (E_{ft}) was used in the transverse factor (η_T).

2.5 Ning Pan Model (1996)

The difficulty of controlling fiber orientation in three dimensions is one of the main reasons why three-dimensional random fiber composite models are rarely used in practice. In this case, the polar and azimuthal angles do not influence the fiber orientation. Therefore, Eq. (12) [38] is derived from the normalization condition.

$$E_c^{3D} = E_f\frac{V_f}{2\pi} + E_m\left(1 - \frac{V_f}{2\pi}\right) \tag{12}$$

Where E_m is the Young's modulus of the matrix, E_f is the Young's modulus of the fiber, V_f is the fiber volume fraction.

2.6 Piggot Model (1980)

Piggott proposed a theoretical model for estimating the elastic modulus of fiber-reinforced composite materials with randomly oriented fibers in three dimensions. His approach accounts for the statistical distribution of fiber orientations within the matrix and the contribution of each orientation to the overall stiffness of the composite, as expressed in Eq (13) [39].

$$E_c = \left(\frac{1}{5}\right).E_f.V_f + E_m.V_m \tag{13}$$

Where E_f is the elastic modulus of the fiber, E_m is the elastic modulus of the matrix, V_f is the fiber volume fraction, and V_m is the matrix volume fraction.

2.7 Lavngood and Goettler Model (1987)

Lavngood and Goettler developed a micromechanical model to estimate the effective elastic modulus (E_c) of randomly oriented short-fiber composites. For two-dimensional random fiber distributions, they proposed the Reuss type expression given in Eq (14) [40].

$$E_c = \frac{24.E_1.E_2}{(7.E_2 + 17.E_1)} \tag{14}$$

Where E_1 an E_2 are calculated as follows [40]:

$$E_1 = E_m + V_f\left(E_f - E_m\right) \tag{15}$$

E_m and E_f signify the Young's modulus of the matrix and the fiber, respectively; V_f represents the volume fraction of the fiber; R signifies the ratio of the transverse modulus of the fiber to that of the matrix.

$$E_2 = E_m \left[\frac{\{2V_f(R-1) + (R+2)\}}{\{V_f(1-R) + (R+2)\}} \right] \tag{16}$$

E_m and E_f signify the Young's modulus of the matrix and the fiber, respectively; V_f represents the volume fraction of the fiber; R signifies the ratio of the transverse modulus of the fiber to that of the matrix.

3. Critical Length (L_c)

The reinforcement of nanocomposites with discontinuous fibers is contingent upon their critical length (L_c). The critical length represents the shortest fiber length capable of enduring the maximum stress applied at its midpoint. The critical length is determined using Eq. (17) [41,42].

$$\frac{L_c}{d_f} = \frac{\sigma_f}{2K\tau_{my}} \tag{17}$$

In where d_f denotes the average CNT diameter and σ_f denotes their tensile strength; τ_{my} denotes the matrix shear stress, which is approximately 60 to 80 MPa (or about half of the yield strength), and K denotes the load transfer efficiency. The value of K is taken as 1 for d_f =0.08 μm and σ_f =60GPa [43]. assuming an effective adhesion contact between the polymer matrix and the CNTs. Based on these parameters, the calculated critical length is (L_c = 30 μm). This value represents the theoretical critical length required for efficient stress transfer and is considered only as a reference parameter. It does not correspond to the actual CNT length used in the numerical model. In the present study, the CNTs introduced in the RVE have an average length of (0.3 μm = 300 nm) [44-46] and an outer diameter of (0.08 μm) [44,47], corresponding to an aspect ratio of (L/D = 3.75). The use of shortened CNTs allows a realistic representation of CNT distribution within the RVE and enables the investigation of the effects of CNT orientation and volume fraction on the effective elastic modulus of the nanocomposite.

4. Finite Element Modeling

4.1 Objective

In this study, the influence of short CNT orientation on the effective elastic modulus (E_c) was investigated using a representative volume element (RVE). The numerical simulations were performed using the finite element method (FEM) implemented in Cast3M through the GIBIANE programming language [48,49]. The random fiber orientations used in each model are summarized in Table 1 below.

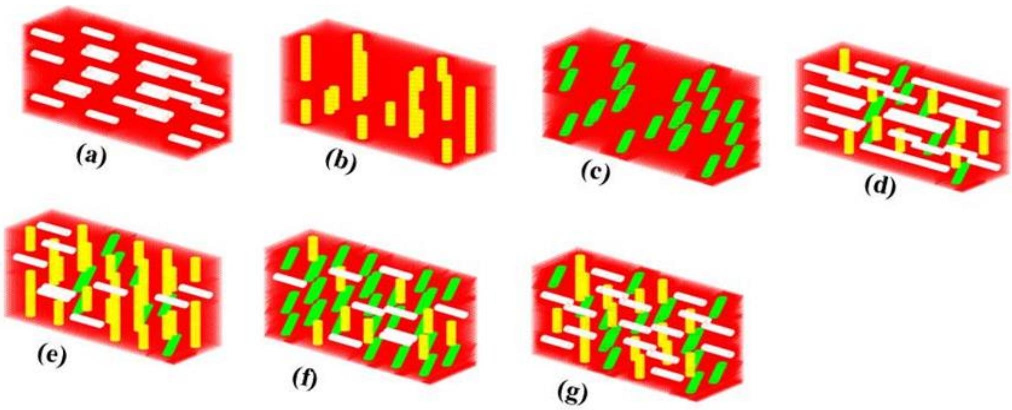

Fig. 1. The models of RVEs : (a) horizontal fibers, (b) vertical fibers ,(c) inclined fibers,(d,e,f and g) random fibers

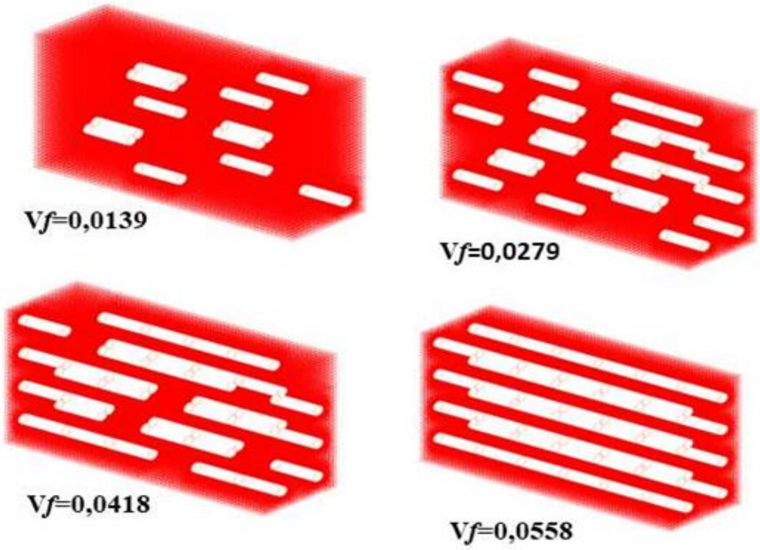

Fig. 2. RVEs (a) for volume fraction (1.39%,2.79%,4.18 % and 5.58%)

Table 1. Distribution and orientation of Carbon Nanotubes Fibers.

RVEs	Percentage CNTs fibers
(d)	62.5%H, 18.75%V, 18.75%I
(e)	62.5%V, 18.75%H 18.75%I
(f)	62.5%I, 18.75%V, 18.75%H
(g)	33.33%H, 33.33%V, 33.33%I

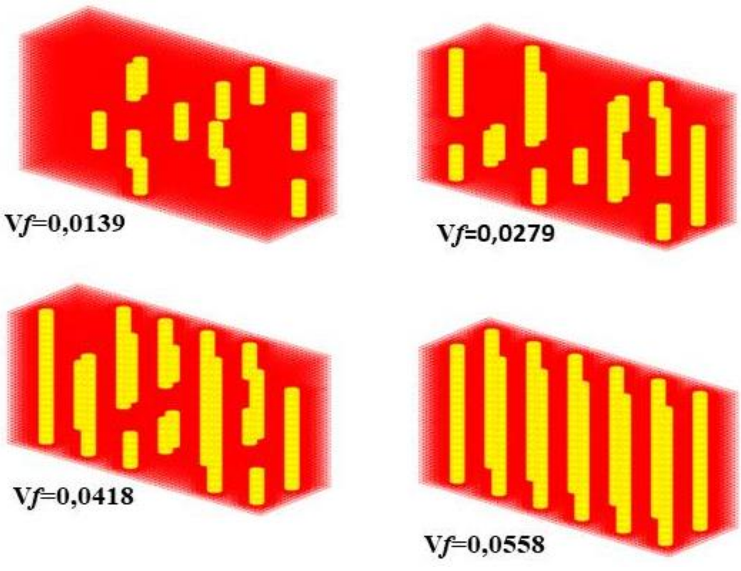

Fig. 3. RVEs (b) for volume fraction (1.39%,2.79%,4.18 % and 5.58%)

Two parameters were considered in this investigation. The first parameter was the CNT orientation. Seven orientation configurations were analyzed, resulting in seven representative volume elements (RVEs), as illustrated in Figure 1. The second parameter was the CNT volume fraction. For RVE models (a), (b), and (c), four volume fractions (1.39%, 2.79%, 4.18%, and 5.58%) were investigated, as shown in Figures (2-4). Models (d), (e), (f), and (g) correspond to four RVEs containing randomly distributed short CNTs with the same volume fraction (V_f). Each RVE includes a random mixed orientation of horizontal (H), vertical (V), and inclined (I) CNTs with different relative proportions. In the present study, the term "random orientation" refers to this mixed and controlled combination of the three prescribed CNT orientations and does not represent a continuous statistically random orientation distribution in three-dimensional space. This approach allows the effects of CNT orientation and spatial distribution on the effective elastic modulus (E_c) to be systematically investigated.

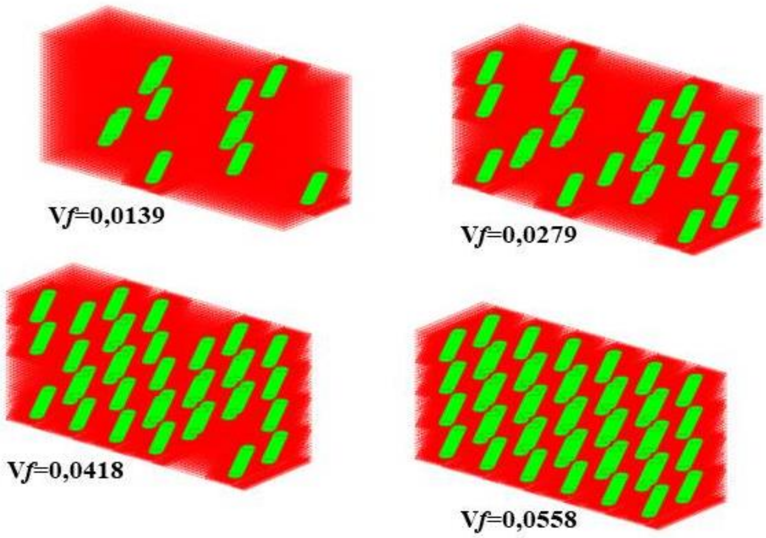

Fig. 4. RVEs (c) for volume fraction (1.39%,2.79%,4.18 % and 5.58%)

4.2 Materials and Characterizations

The nanocomposite is made up of a polymer matrix reinforced with short carbon nanotube fibers and is widely used in various sectors, notably medical devices and electronics [50, 51]. Tables 2 and 3 provide a summary of the main mechanical properties of the polymer/CNT nanocomposite.

Table 2. Mechanical properties of the polymer [52]

Constituent	Young's modulus (GPa)	Poisson's ratio (ν)	Density (kg/ m³)
Polymer	3.2	0.3	950

Table 3. characterizations constants of carbon nanotubes (CNTs) [53]

E_1(GPa)	E_2=E_3(GPa)	G_{12}=G_{13}(GPa)	G_{23}(GPa)	$\nu_{13}=\nu_{12}$	ν_{23}
2100	420	790	130	0.1716	0.595

4.3 Representative Volume Element (RVE)

A representative volume element (RVE) was employed to model the CNT/polymer nanocomposite. The geometrical dimensions of the RVE are presented in Table 4. Figure 5 illustrates a representative RVE containing vertically aligned CNTs embedded in the polymer matrix. The dimensions of (1.8× 0.6 ×1.2 μm) define the computational cell used in the present parametric study. These dimensions were selected to accommodate the (0.3 μm) CNT inclusions, together with the prescribed volume fractions and orientation configurations.

Table 4. RVE details

Parameter of RVE	
L(μm)	1.8
W(μm)	0.6
H(μm)	1.2
Diameter of CNT(nm)	80

The adopted size therefore corresponds to a representative configuration consistently used for all analyzed cases, rather than to a critical RVE size established through a systematic convergence study; accordingly, these dimensions should not be interpreted as a demonstrated critical RVE size.

The conclusions of the present study are therefore limited to the modeled cell. A future RVE study should progressively increase both the domain size and the number of independent random realizations until the variation in the mean effective modulus and the associated dispersion fall below a predefined tolerance.

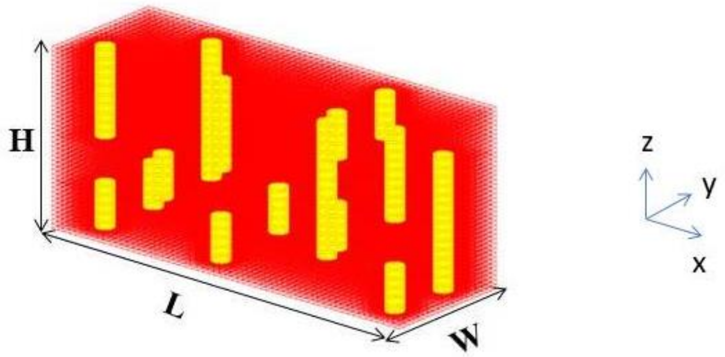

Fig. 5. RVE with short CNT fibres oriented vertical

4.4 Calculation of The Elastic Modulus by Modeling

In this work, the effective elastic modulus (E_c) of the CNT/polymer nanocomposite is calculated for different CNT volume fractions (V_f) using a numerical method. The flowchart of the proposed computational procedure is shown in Figure 6.

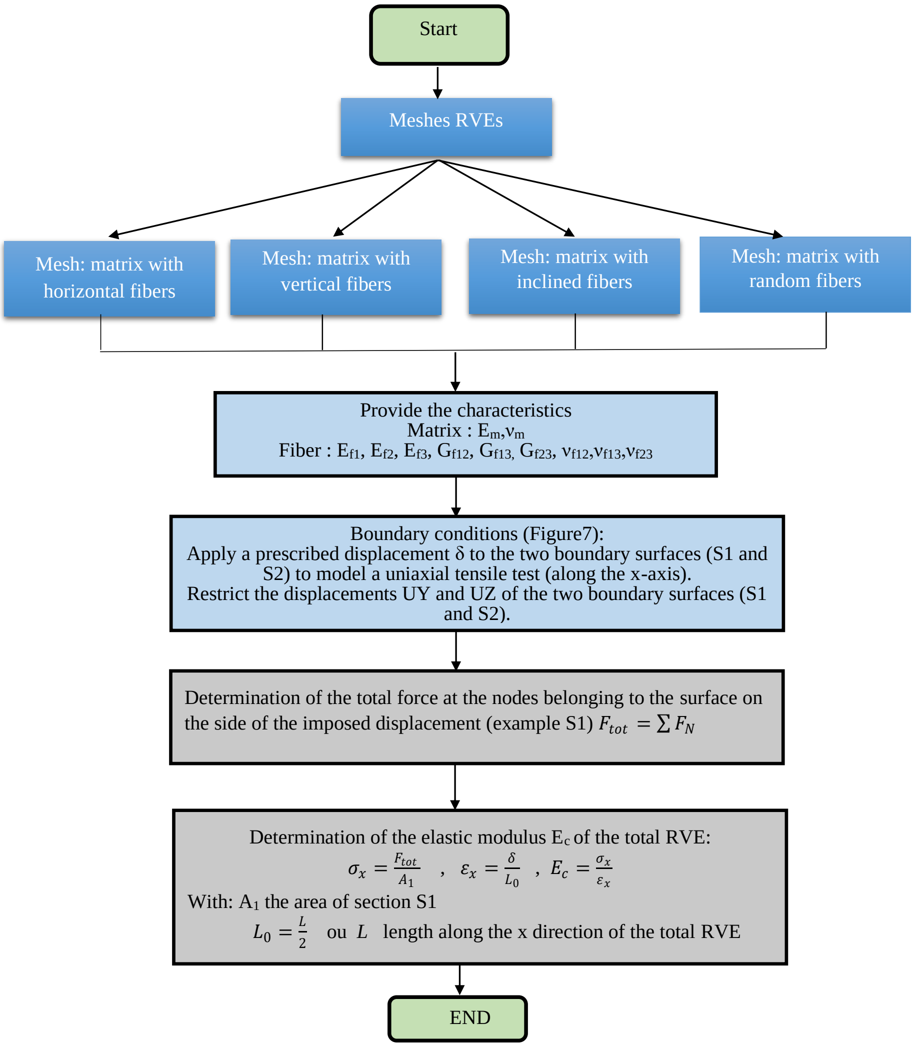

Fig. 6. Flowchart illustrating the procedure for evaluating the elastic modulus

4.5 Loading and Boundary Conditions

In this study, prescribed displacements were applied to the two opposite faces (S1 and S2) of the representative volume element (RVE) along the loading direction. A symmetric uniaxial tensile loading condition was imposed by applying equal and opposite displacements to these two faces, with (U_x=+ δ) on face S1 and (U_x =- δ) on face S2. The transverse displacement components were constrained by setting (U_y=0) and (U_z=0) to prevent rigid-body motion and ensure numerical stability during the simulations. As illustrated in Figure (7), this loading configuration produces deformation along the (x)-direction.

Since the RVE was generated from a non-periodic random distribution of short carbon nanotubes, the adopted constraints correspond to uniform kinematic boundary conditions rather than periodic boundary conditions. The imposed transverse displacement constraints partially suppress transverse displacement fluctuations and may therefore lead to a certain overestimation of the effective elastic modulus compared with that obtained using a fully periodic homogenization scheme. Nevertheless, because the same boundary conditions were applied to all investigated RVEs, the relative comparisons of the effects of CNT orientation and volume fraction on the effective elastic modulus remain consistent and meaningful.

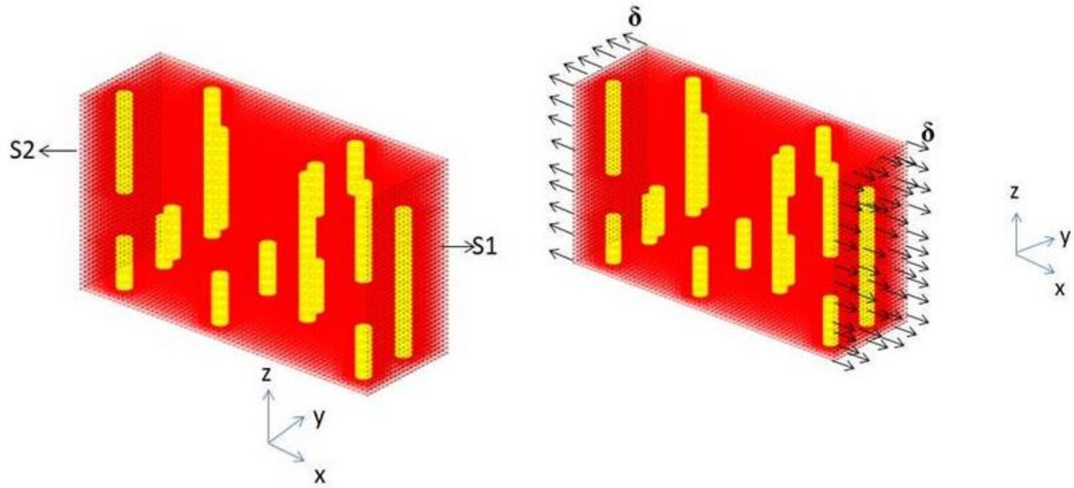

Fig. 7. The displacement δ applied to the RVE

5. Results and Discussion

5.1 The Influence of the Short Fiber Orientation on the Elastic Modulus E_c

Figure 8 presents the simulation results for the effective elastic modulus (E_c) obtained from the three representative volume elements (RVEs a, b, and c). The results clearly demonstrate the combined influence of CNT orientation and volume fraction on the mechanical behavior of the CNT/polymer nanocomposite. As expected, the elastic modulus increases with increasing CNT volume fraction for all orientation configurations, owing to the higher contribution of the stiff CNT reinforcement and the enhanced load-bearing capacity of the composite.

Among the investigated configurations, the RVE containing horizontally aligned CNTs (parallel to the loading direction) exhibits the highest elastic modulus. This behavior can be attributed to the efficient transfer of the applied tensile load from the polymer matrix to the CNTs, which possess a significantly higher intrinsic stiffness. When the reinforcement is aligned with the loading direction, the axial stiffness of the CNTs is fully exploited, resulting in a more effective stress transfer and a greater contribution to the overall composite stiffness. For example, the results for RVE (a) show an increase of 9.66% compared to RVE (b) for V_f = 0.0279 and an increase of 11.86% for V_f = 0.0418.

Conversely, the RVE with vertically oriented CNTs exhibits the lowest elastic modulus under horizontal tensile loading. In this configuration, the reinforcement is oriented perpendicular to the applied load, preventing the CNTs from effectively carrying axial stresses. Consequently, the polymer matrix bears most of the applied load, leading to a lower overall stiffness. For instance,the results for RVE (b) show a decrease of 3.13% compared to RVE (c) for V_f = 0.0139 and a decrease of 4.19% for V_f = 0.0558.The inclined orientation provides an intermediate mechanical response because only a portion of the applied load is transmitted along the CNT axis, while the remaining component is accommodated by the polymer matrix. Therefore, the reinforcing efficiency decreases as the CNT orientation deviates from the loading direction. Overall, these findings confirm that both CNT orientation and volume fraction are key parameters governing the effective elastic modulus of CNT/polymer nanocomposites. Their combined influence is primarily controlled by the efficiency of stress transfer across the CNT/matrix interface and the ability of the aligned CNT network to resist the applied deformation.

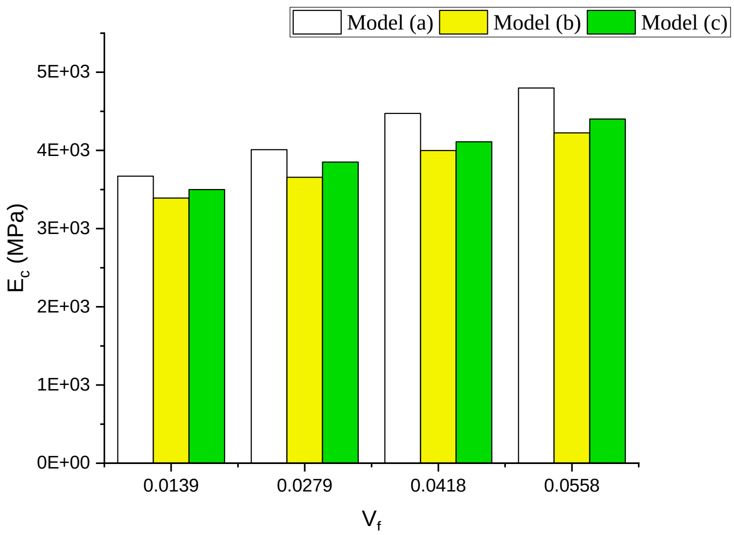

Fig. 8. Comparison between E_c obtained

Figure 9 illustrates the influence of CNT orientation distribution on the effective elastic modulus (E_c) while maintaining a constant CNT volume fraction (V_f = 0.0558). Four representative volume elements (RVEs (d-g)) with identical CNT content but different proportions of horizontal (H), vertical (V), and inclined (I) CNTs were analyzed to isolate the effect of fiber orientation. The results show that RVE (d), containing 62.5% horizontally oriented CNTs, exhibits the highest elastic modulus, whereas RVE (e), with 62.5% vertically oriented CNTs, gives the lowest value. RVEs (f) and (g), containing predominantly inclined CNTs and an equal distribution of orientations, respectively, exhibit intermediate stiffness.

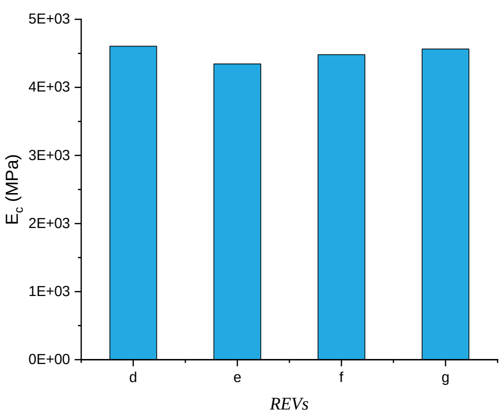

Fig. 9. Comparison between E_c obtained For V_f = 0.0558

The superior performance of RVE (d) is attributed to the alignment of most CNTs with the loading direction, which promotes efficient stress transfer from the polymer matrix to the high-stiffness CNTs. In contrast, vertically oriented CNTs contribute less to load carrying under tensile loading because they are nearly perpendicular to the applied stress. The inclined and uniformly distributed orientations provide only partial reinforcement, resulting in intermediate elastic modulus values.These results demonstrate that, even at a constant CNT volume fraction, the elastic modulus strongly depends on the orientation distribution of CNTs. Increasing the proportion of CNTs aligned with the loading direction significantly improves the reinforcing efficiency and the overall stiffness of the nanocomposite.

5.2 Normal Stress Distribution

5.2.1 Normal Stress Distribution σ_{xx}

- Figures 10a, 10b, and 10c illustrate the distribution of normal stress σ_{xx} within the representative volume element (RVE (a)) for a CNT volume fraction of V_f=0.0558.
- Figures 11a, 11b, and 11c illustrate the normal stress distribution σ_{xx} in the representative volume element (RVE(b)) for a volume fraction V_f=0.0558.
- Figures 12a, 12b, and 12c illustrate the normal stress distribution σ_{xx} in the representative volume element (RVE (c)) with a volume fraction V_f =0.0558.
- Figures 13a, 13b, and 13c illustrate the normal stress distribution σ_{xx} in the representative volume element (RVE (g)) with inclined fibers for a volume fraction V_f=0.0558.

5.2.2 Normal Stress Distribution σ_{yy}

- Figures 14a, 14b, and 14c illustrate the normal stress distribution σ_{yy} in(RVE (a)) for V_f = 0.0558.
- The distribution of normal stress σ_{yy} within (RVE (b)) for a CNT volume fraction of V_f=0.0558 is illustrated in Figures 15a, 15b, and 15c.
- Figures 16a, 16b, and 16c illustrate the normal stress distribution σ_{yy} in (RVE (c)) for V_f = 0.0558.
- As an example, the normal stress distribution σ_{yy} in (RVE (g)) for V_f = 0.0558 is shown in Figures 17a, 17b, and 17c.

5.2.3 Normal Stress Distribution σ_{zz}

- Figures 18a, 18b, and 18c illustrate the normal stress distribution σ_{zz} in the representative volume element (RVE (a)) for a volume fraction V_f =0.0558
- Figures 19a, 19b, and 19c illustrate the normal stress distribution σ_{zz} in the representative volume element (RVE (b)) with a volume fraction V_f =0.0558.
- Figures 20a, 20b, and 20c illustrate the normal stress distribution σ_{zz} in (RVE (c)) for V_f = 0.0558.
- Figures 21a, 21b, and 21c illustrate the typical stress distribution σ_{zz} in (RVE (g)) for V_f = 0.0558.

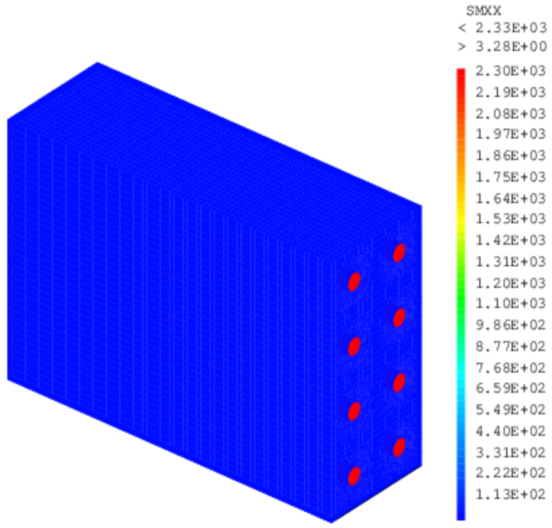

(a) Stress σ_{xx} distribution in the matrix and fibers

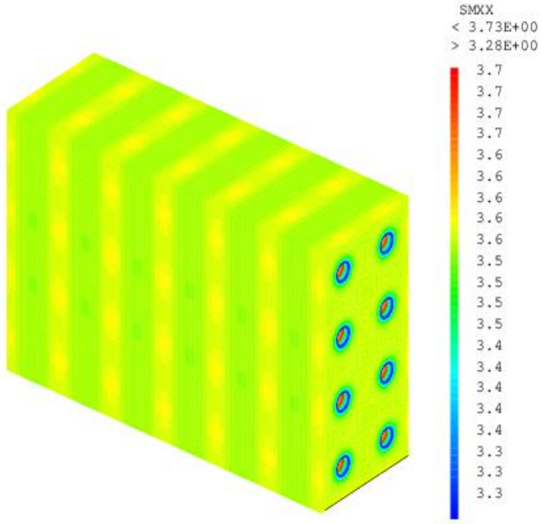

(b) Stress σ_{xx} distribution in the matrix

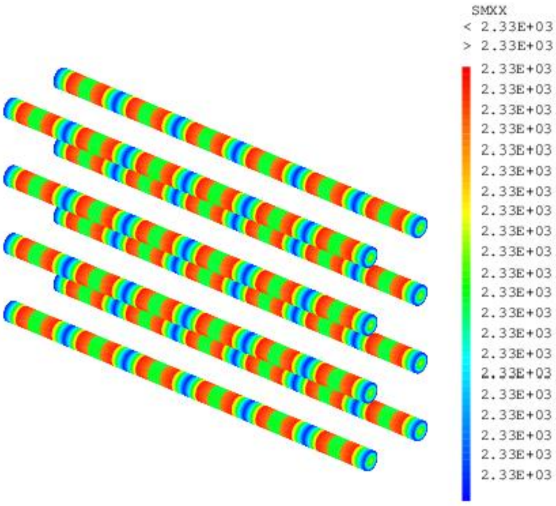

(c) Stress σ_{xx} distribution in the fibers

Fig. 10. Stress σ_{xx} distribution for (RVE (a))

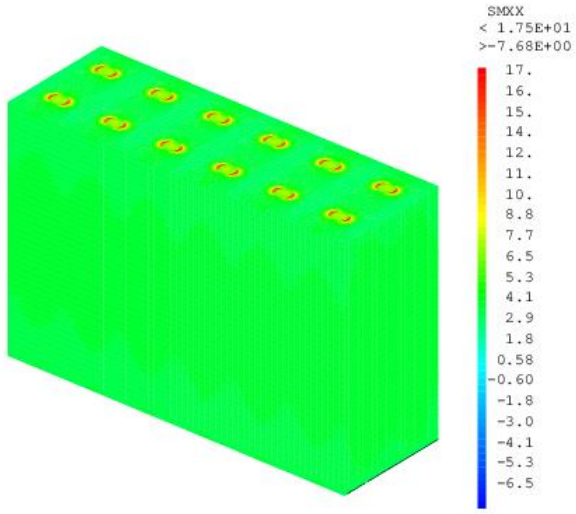

(a) Stress σ_{xx} distribution in the matrix and fibers

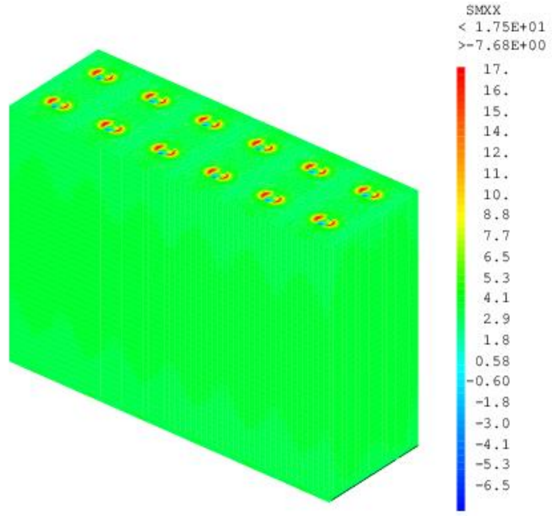

(b) Stress σ_{xx} distribution in the matrix

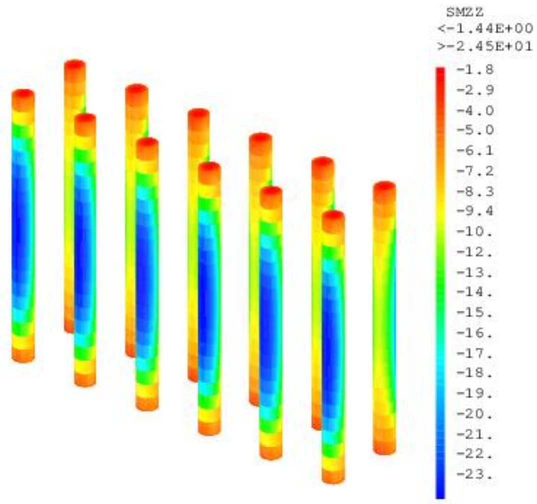

(c) Stress σ_{xx} distribution in the fibers

Fig. 11. Stress σ_{xx} distribution for (RVE (b))

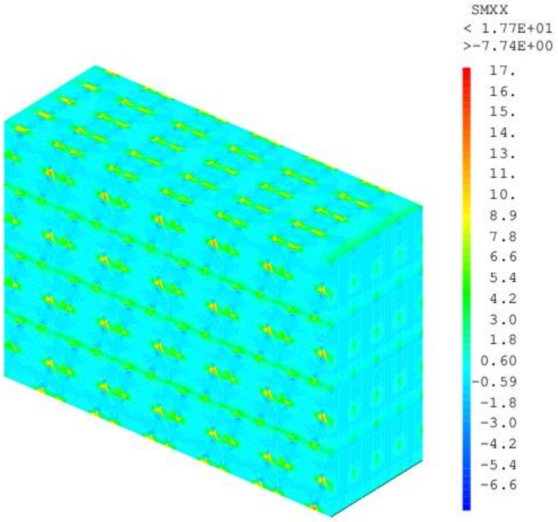

(a) Stress σ_{xx} distribution in the matrix and fibers

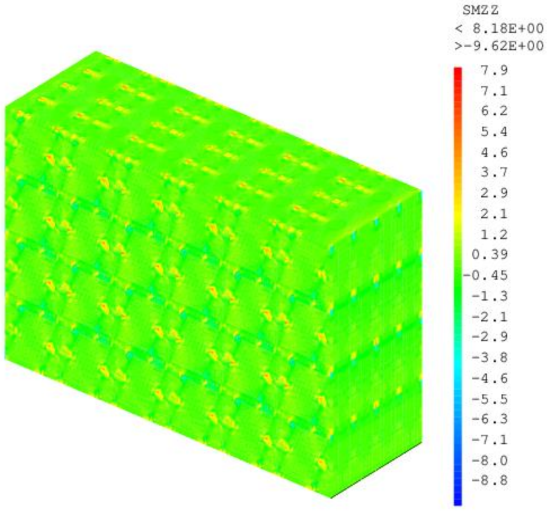

(b) Stress σ_{xx} distribution in the matrix

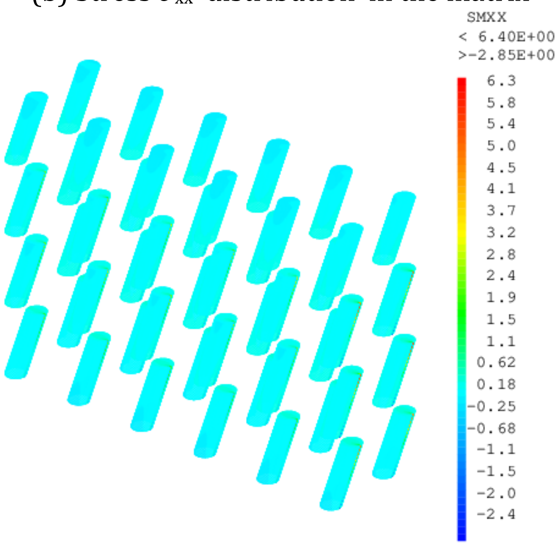

(c) Stress σ_{xx} distribution in the fibers

Fig. 12. Stress σ_{xx} distribution for (RVE (c))

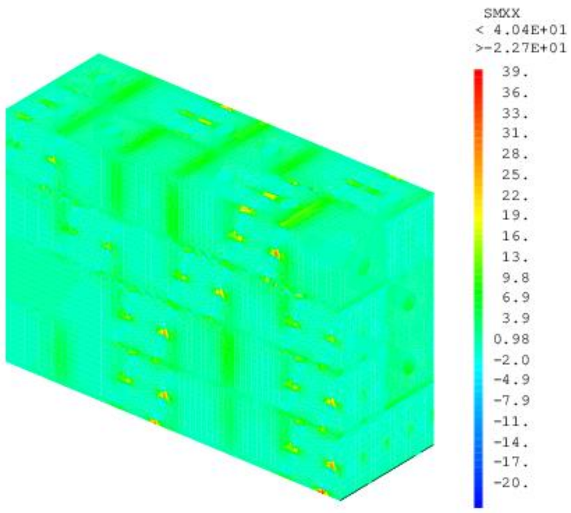

(a) Stress σ_{xx} distribution in the matrix and fibers

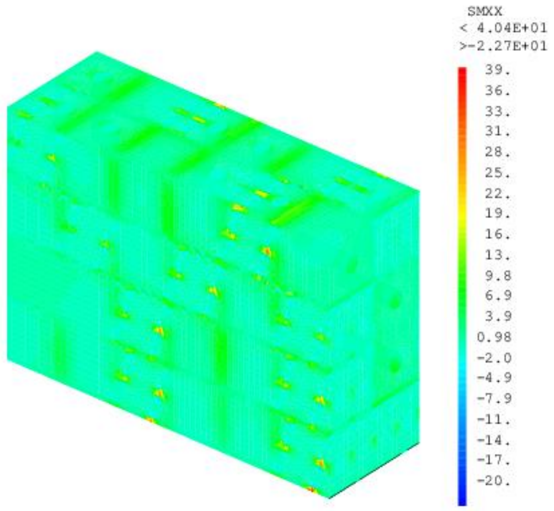

(b) Stress σ_{xx} distribution in the matrix

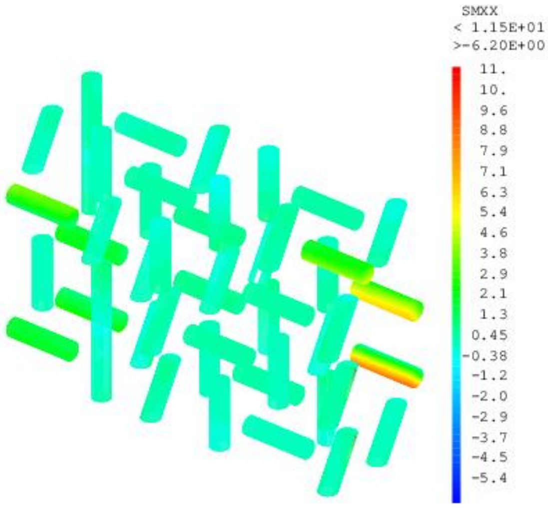

(c)Stress σ_{xx} distribution in the fibers

Fig. 13. Stress σ_{xx} distribution for (RVE (g))

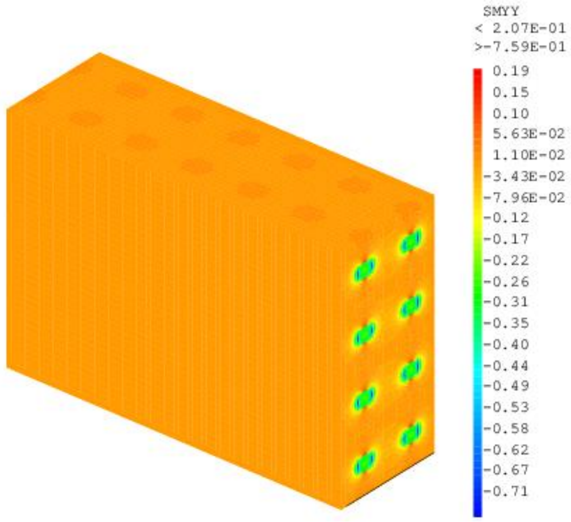

(a) Stress σ_{yy} distribution in the matrix and fibers

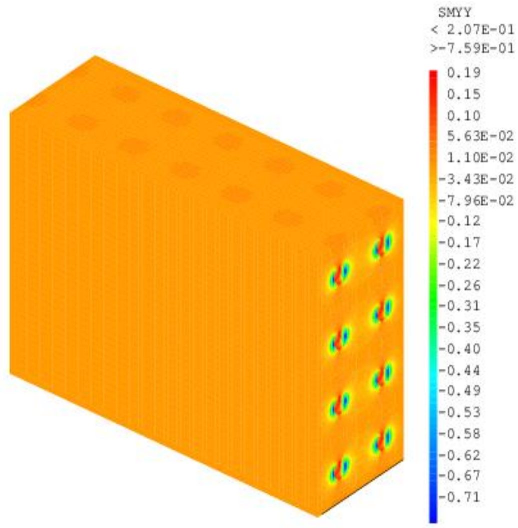

(b) Stress σ_{yy} distribution in the matrix

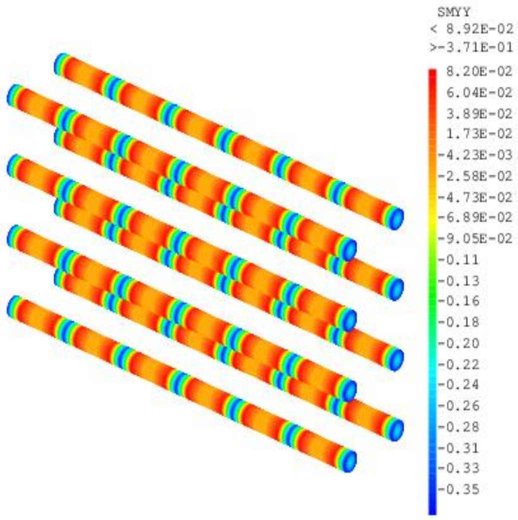

(c)Stress σ_{yy} distribution in the fibers

Fig. 14. Stress σ_{yy} distribution for (RVE (a))

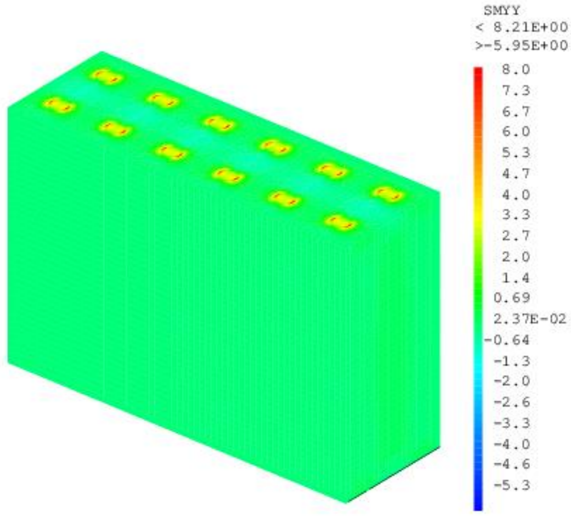

(a) Stress σ_{yy} distribution in the matrix and fibers

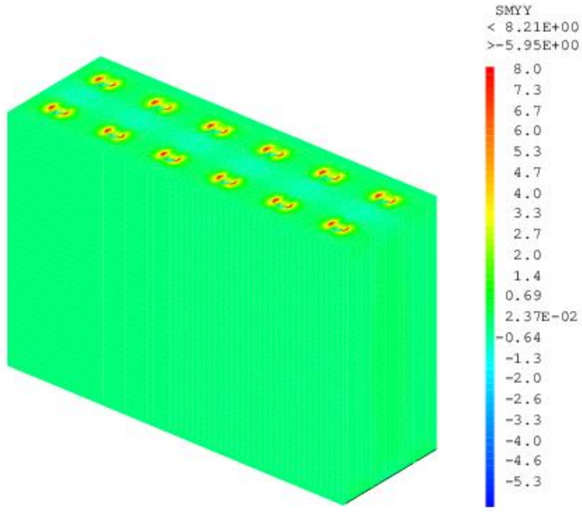

(b) Stress σ_{yy} distribution in the matrix

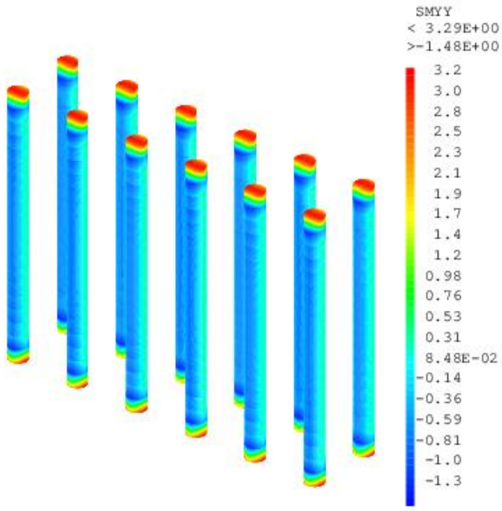

(c) Stress σ_{yy} distribution in the fibers

Fig. 15. Stress σ_{yy} distribution for (RVE (b))

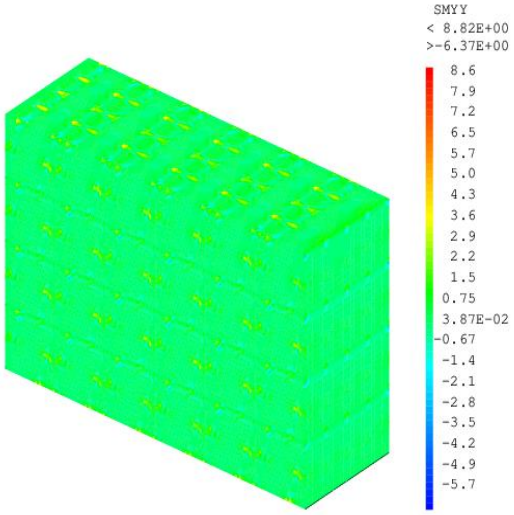

(a) Stress σ_{yy} distribution in the matrix and fibers

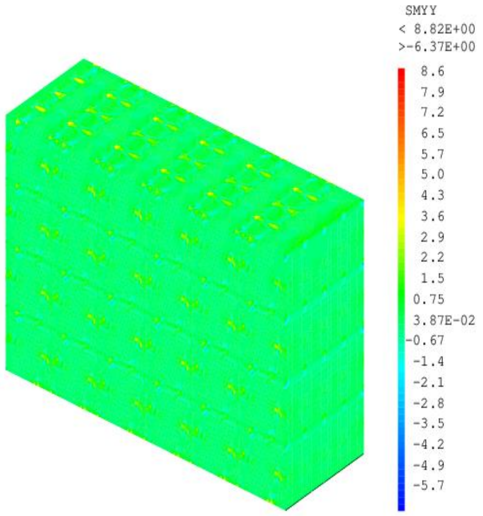

(b) Stress σ_{yy} distribution in the matrix

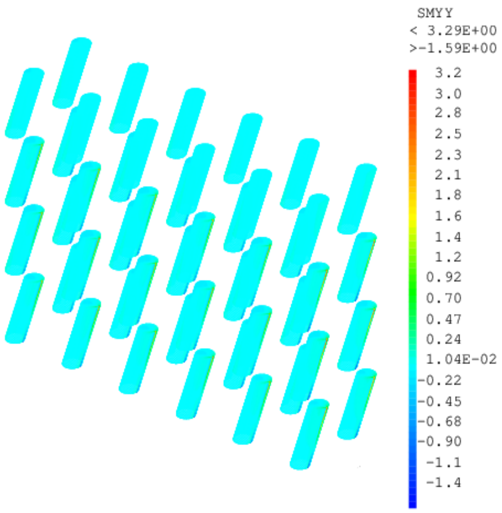

(c) Stress σ_{yy} distribution in the fibers

Fig. 16. Stress σ_{yy} distribution for (RVE (c))

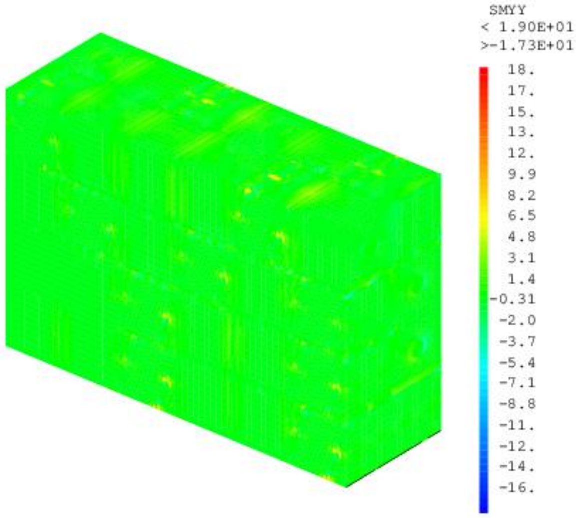

(a) Stress σ_{yy} distribution in the matrix and fibers

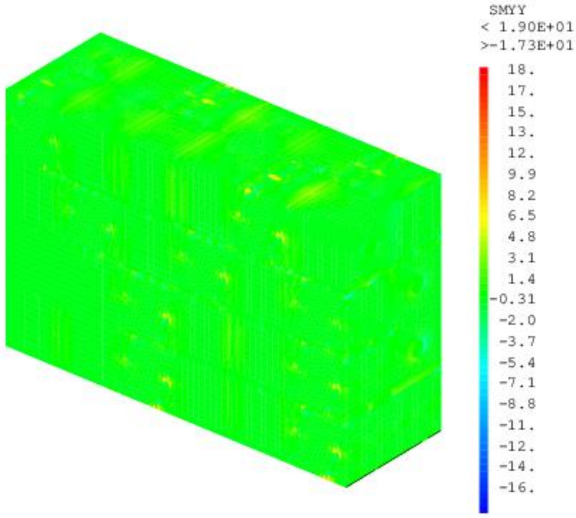

(b) Stress σ_{yy} distribution in the matrix

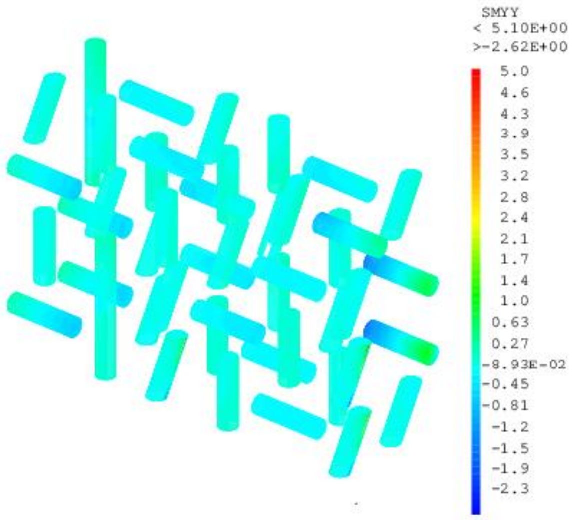

(c) Stress σ_{yy} distribution in the fibers

Fig. 17. Stress σ_{yy} distribution for (RVE (g))

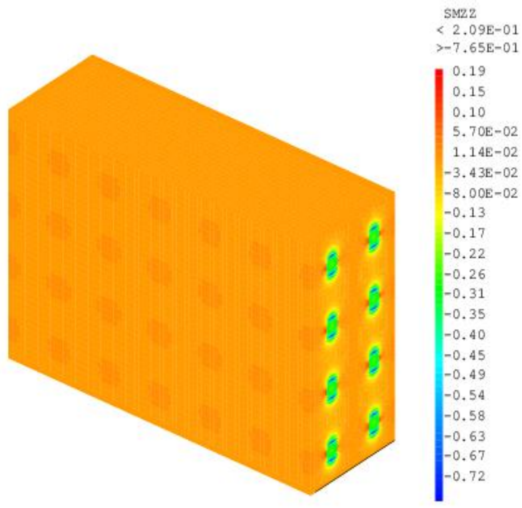

(a) Stress σ_{zz} distribution in the matrix and fibers

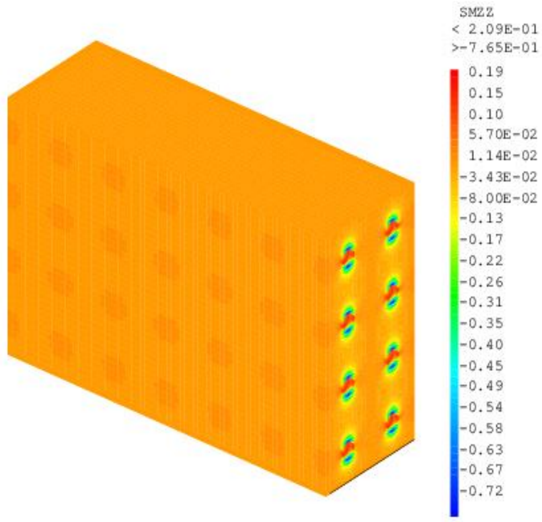

(b) Stress σ_{zz} distribution in the matrix

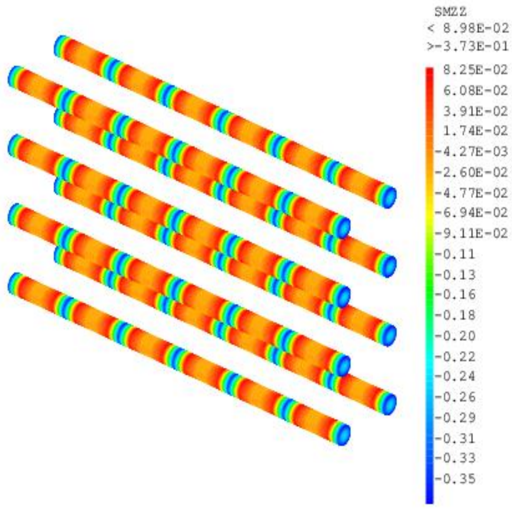

(c)Stress σ_{zz} distribution in the fibers

Fig. 18. Stress σ_{zz} distribution for (RVE (a))

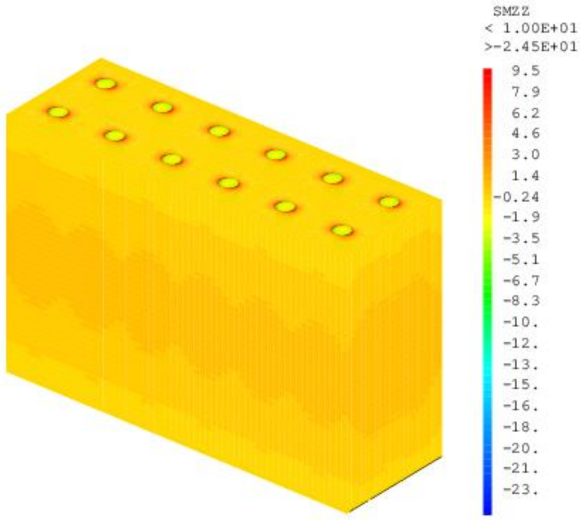

(a) Stress σ_{zz} distribution in the matrix and fibers

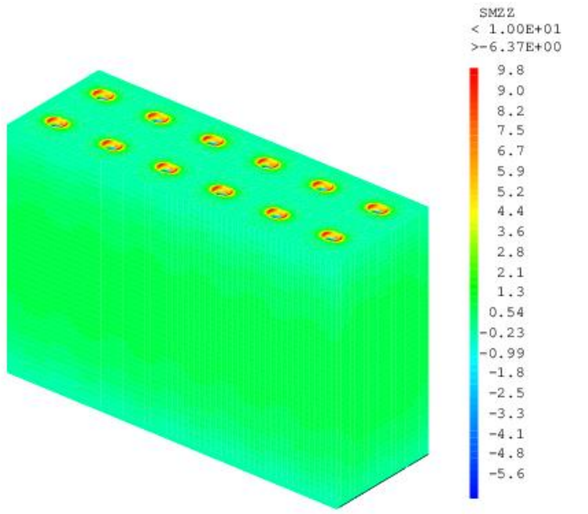

(b) Stress σ_{zz} distribution in the matrix

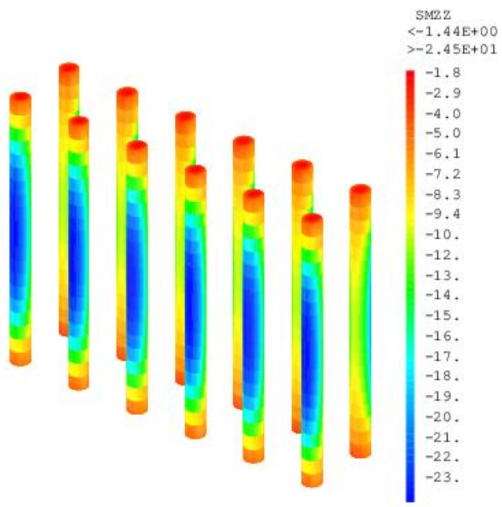

(c) Stress σ_{zz} distribution in the fibers

Fig. 19. Stress σ_{zz} distribution for (RVE (b))

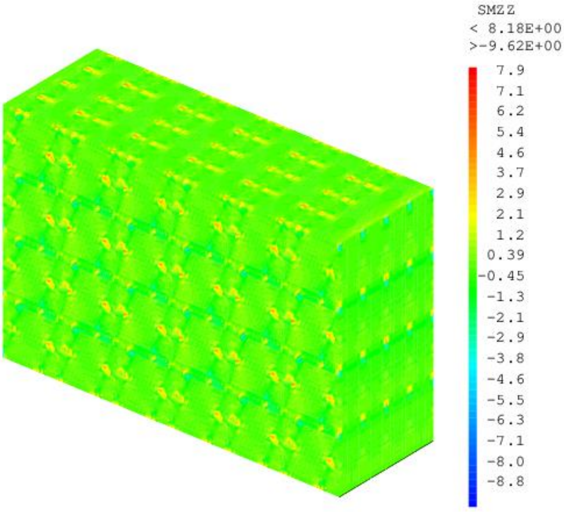

(a) Stress σ_{zz} distribution in the matrix and fibers

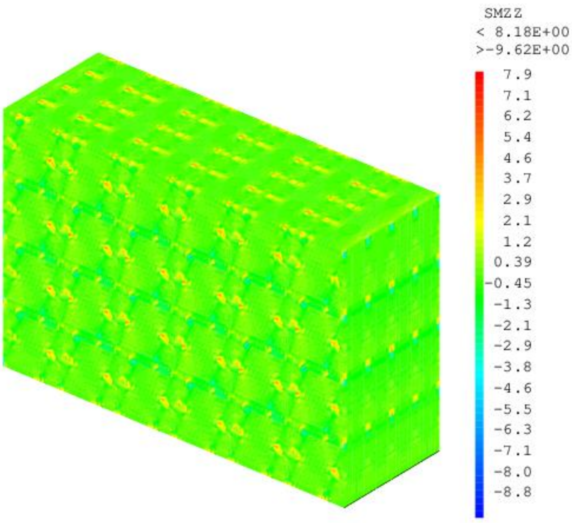

(b) Stress σ_{zz} distribution in the matrix

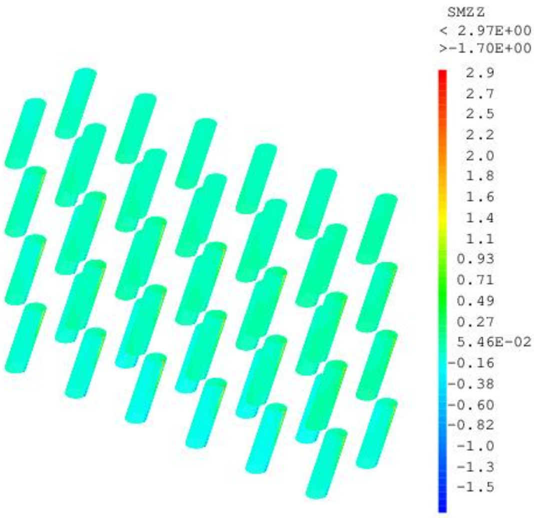

(c)Stress σ_{zz} distribution in the fibers

Fig. 20. Stress σ_{zz} distribution for (RVE (c))

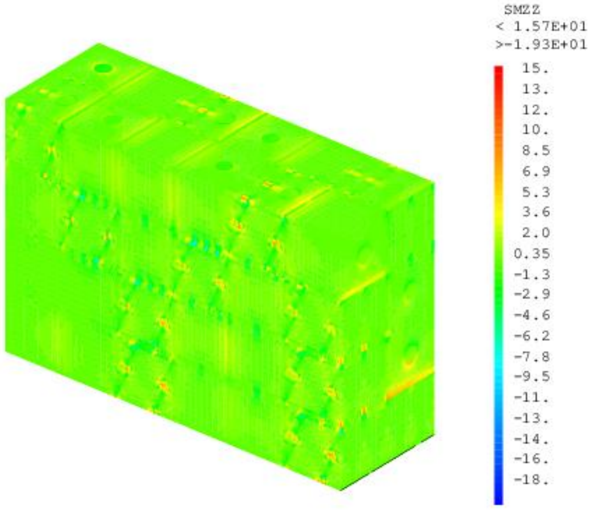

(a) Stress σ_{zz} distribution in the matrix and fibers

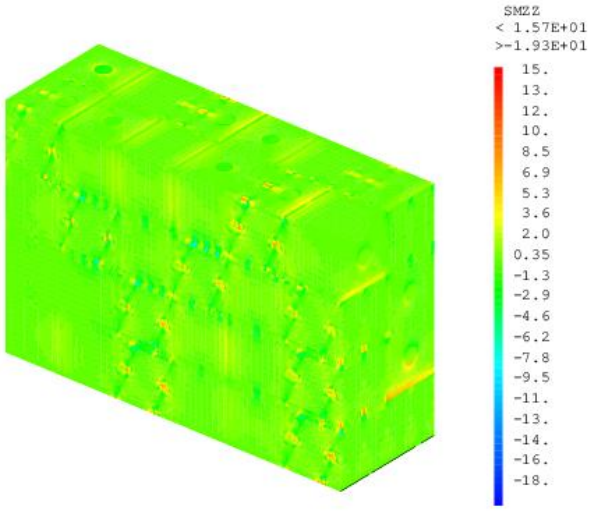

(b) Stress σ_{zz} distribution in the matrix

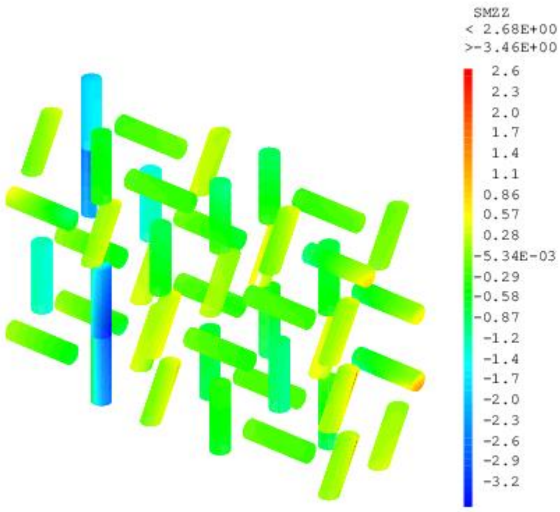

(c) Stress σ_{zz} distribution in the fibers

Fig. 21. Stress σ_{zz} distribution for (RVE (g))

5.3 Comparison Between the Obtained Values and The Values Calculated Using Analytical Models

5.3.1 The Case of A Horizontal Orientation of Short Fibers

Figure 22 compares the elastic modulus (E_c) obtained from the FEM simulations with the analytical models for horizontally oriented CNTs. The results show that E_c increases with increasing CNT volume fraction, confirming the reinforcing effect of CNTs. A good agreement is observed between the FEM results and the Halpin-Tsai and Cox models for V_f=0.0139-0.0279, while the results are closer to the Lavngood and Goettler model at V_f=0.0558. The differences between the numerical and analytical predictions are mainly related to the idealized assumptions of the analytical models compared with the actual CNT distribution considered in the FEM simulations.

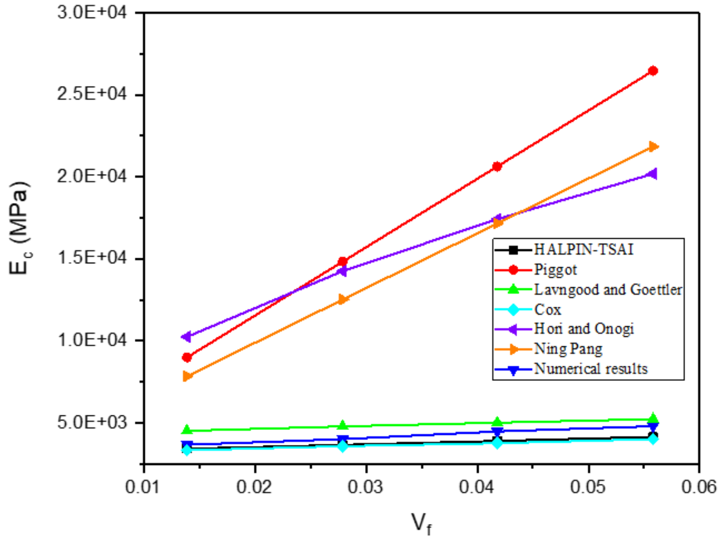

Fig. 22. Comparison of the values determined by the analytical models for short horizontal fibers

5.3.2 The Case of a Horizontal Orientation of Short Fibers

Figure 23 compares the elastic modulus (E_c) obtained from the FEM simulations with the analytical models for vertically oriented CNTs. The results show a linear increase in (E_c) with increasing CNT volume fraction, confirming the contribution of CNT reinforcement to the composite stiffness.

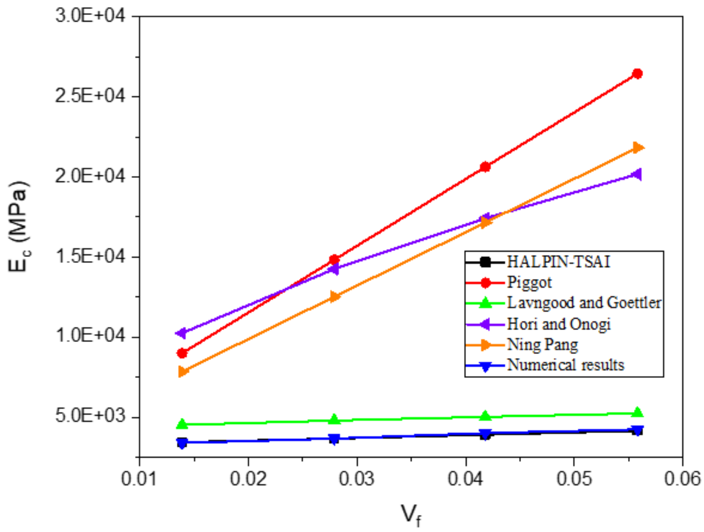

Fig. 23. Comparison of the values determined by the analytical models for short vertical fibers

The FEM predictions are lower than those of the analytical models over the investigated range (V_f = 0.0139-0.0558), while a relatively good agreement is observed with the Halpin–Tsai model. The differences can be attributed to the simplifying assumptions of the analytical models compared with the numerical approach, which considers the actual CNT distribution within the RVE.

5.3.3 The Case of An Inclined Orientation of Short Fibers

In this case (Figure 24), the results obtained confirm those previously observed regarding the relationship between the volume fraction and the elastic modulus. A proportional relationship is clearly established between these two parameters: the modulus of elasticity increases proportionally with the increase in volume fraction.for volume fraction (V_f) values ranging between 0.0139 and 0.0558, the obtained results are close to the values from the Halpin-Tsai model.

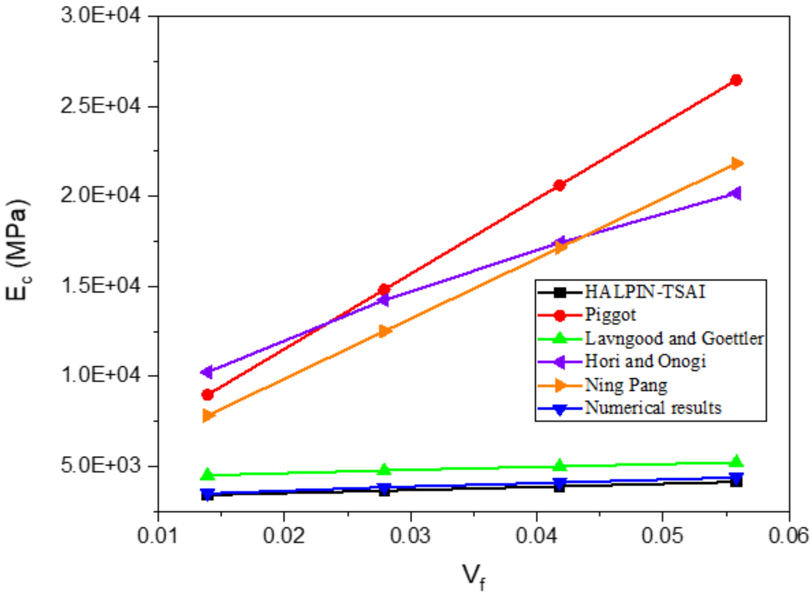

Fig. 24. Comparison of the values determined by the analytical models for short inclined fibers.

The relative error between the FEM results and the Halpin-Tsai analytical model was calculated using Eq (18) to quantitatively assess the agreement between the two approaches.

$$Error(\%) = \frac{|E_{FEM} - E_{HT}|}{E_{HT}} x100 \tag{18}$$

The average relative error was 11.78% for the horizontal orientation, 4.73% for the inclined orientation, and 2.26% for the vertical orientation. The overall average relative error was 6.26%, confirming the good agreement between the FEM predictions and the Halpin-Tsai analytical model.

5.3.4 The Case of Random Orientation of Short Fibers

Figure 25 represents a comparison between the obtained results and the analytical models for V_f = 0.0558, where we note that the results obtained for four different models (d, e, f, and g) are very close to the Halpin-Tsai model and the Lavngood and Goettler model. As for the three models (Hori and Onogi, Nin Pang, and Piggot), they often assume ideal conditions for short fibers, such as perfect adhesion between the fibers and the matrix, uniform distribution, and ideal transfer constraints. These assumptions lead to a value of the elastic modulus that is much higher than that observed in practical experiments, where fiber spacing, non-ideal adhesion, and the presence of voids and impurities are important factors.

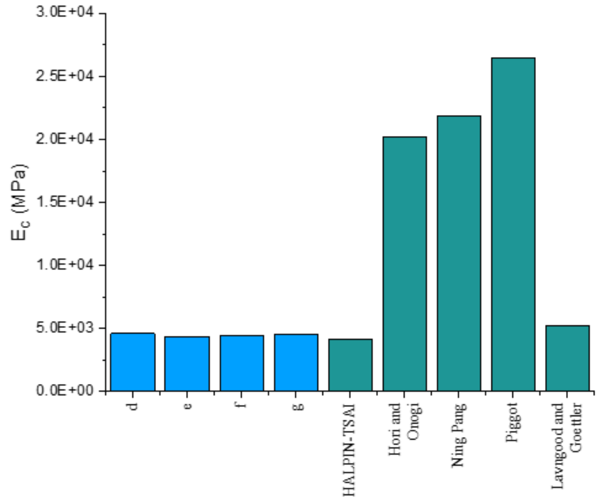

Fig. 25. Comparison of the values determined by the analytical models for short random fibers for V_f =0.0558.

6. Conclusions

This study investigated the effect of CNT orientation distribution and volume fraction on the effective elastic modulus (E_c) of CNT/polymer nanocomposites using a three-dimensional finite element method (FEM) combined with a micromechanical approach. Unlike studies that only consider the influence of CNT content, the present work focuses on the role of reinforcement arrangement and orientation within the representative volume element (RVE). Several CNT configurations, including horizontal, vertical, inclined, and randomly distributed orientations, were analyzed and compared with established analytical models to evaluate the reliability of the numerical predictions. The main conclusions obtained from this study are summarized as follows:

- The obtained results demonstrate that CNT orientation is a key parameter controlling the mechanical response of the nanocomposite. The highest elastic modulus values were obtained for horizontally aligned CNTs, where the reinforcement direction is favorable for load transfer. This configuration allows the CNTs to contribute more efficiently to carrying the applied load due to their high axial stiffness. In contrast, vertically oriented CNTs resulted in lower elastic modulus values because their orientation reduces their contribution to resisting the applied deformation. The inclined and randomly distributed configurations exhibited intermediate mechanical behavior, confirming that the orientation distribution of CNTs can significantly modify the reinforcing efficiency even when the CNT volume fraction remains constant.
- The results also confirm that increasing the CNT volume fraction leads to a progressive increase in the elastic modulus of the composite. This improvement is attributed to the higher contribution of the stiff CNT phase and the increased ability of the reinforcement to transfer mechanical loads within the polymer matrix. However, the results indicate that increasing CNT content alone is not sufficient to maximize the mechanical performance, since the orientation and spatial distribution of CNTs play an equally important role in determining the effective stiffness of the nanocomposite.
- The numerical predictions obtained from the FEM simulations showed good agreement with the analytical models. In particular, the Halpin-Tsai model provided close predictions over the investigated volume fraction range, while the Cox and Lavngood-Goettler models also showed satisfactory agreement for specific CNT orientations and volume fractions. The differences observed between FEM and analytical predictions are mainly related to the idealized assumptions used in analytical models compared with the actual CNT distribution considered in the numerical simulations.
- Overall, the present study highlights the importance of controlling CNT orientation and dispersion in the design of CNT/polymer nanocomposites. The proposed numerical approach provides a useful framework for predicting the elastic behavior of such materials

and can support the optimization of composite structures where improved stiffness and mechanical performance are required.

The results presented in this work are numerical predictions cross-checked against analytical micromechanical models. No experimental validation was performed; therefore, the reported elastic modulus values should be interpreted as model-based estimates for the investigated assumptions and parameter range, rather than as experimentally validated material properties.

References

[1] Amraei J, Jam JE, Arab B, Firouz-Abadi RD. Modeling the interphase region in carbon nanotube-reinforced polymer nanocomposites. Polym Compos. 2019;40(S2):E1219-E34. https://doi.org/10.1002/pc.24950

[2] Nurazzi NM, Sabaruddin FA, Harussani MM, Kamarudin SH, Rayung M, Asyraf MRM, et al. Mechanical performance and applications of CNTs reinforced polymer composites—A review. Nanomaterials. 2021;11(9):2186. https://doi.org/10.3390/nano11092186

[3] Ibn Malek I, Sarkar K, Zubair A. Predicting the mechanical properties of pristine and defective carbon nanotubes using a random forest model. Nanoscale Adv. 2024;6(20):5112-32. https://doi.org/10.1039/D4NA00405A

[4] Niu M, Cui C, Tian R, Zhao Y, Miao L, Hao W, et al. Mechanical and thermal properties of carbon nanotubes in carbon nanotube fibers under tension-torsion loading. RSC Adv. 2022;12(46):30085-93. https://doi.org/10.1039/D2RA05360H

[5] Hosseyni Khorasgani SM, Dashtbayazi MR. Mechanical property modeling of aluminium nanocomposite reinforced with carbon nanotubes. Emerg Mater Res. 2019;8(4):574-81. https://doi.org/10.1680/jemmr.19.00001

[6] Kurilich M, Park JG, Degraff J, Wu Q, Liang R. Improvement of electrical and thermal properties of carbon nanotube sheets by adding silver nanowire and MXene for an electromagnetic-interference-shielding property study. Nanomaterials. 2024;14(19):1587. https://doi.org/10.3390/nano14191587

[7] Faghidian SA, Elishakoff I. A consistent approach to characterize random vibrations of nanobeams. Eng Anal Bound Elem. 2023;152:14-21. https://doi.org/10.1016/j.enganabound.2023.03.037

[8] Kumar S. Investigating effect of CNT agglomeration in CNT/polymer nanocomposites using multiscale finite element method. Mech Mater. 2023;183:104706. https://doi.org/10.1016/j.mechmat.2023.104706

[9] Moradi A, Ansari R, Hassanzadeh-Aghdam MK, Jang S. Thermomechanical behavior of carbon nanotube/graphene nanoplatelet-reinforced shape memory polymer nanocomposites: A micromechanics-based finite element approach. Eur J Mech A Solids. 2024;107:105360. https://doi.org/10.1016/j.euromechsol.2024.105360

[10] Faghidian SA, Żur KK, Rabczuk T. Mixture unified gradient theory: A consistent approach for mechanics of nanobars. Appl Phys A. 2022;128:996. https://doi.org/10.1007/s00339-022-06130-7

[11] Elaskalany M, Behdinan K. Stochastic multiscale modeling of electrical conductivity of carbon nanotube polymer nanocomposites: An interpretable machine learning approach. Adv Eng Mater. 2024;26(23):2401233. https://doi.org/10.1002/adem.202401233

[12] Huang HB, Huang ZM, Wan YP. Micromechanical predictions on elastic moduli of a short fiber composite with arbitrary geometric combination. Compos Part A Appl Sci Manuf. 2023;168:107477. https://doi.org/10.1016/j.compositesa.2023.107477

[13] Caliskan U, Gulsen H, Apalak MK. New approach for modeling randomly distributed CNT reinforced polymer nanocomposite with van der Waals interactions. Mech Adv Mater Struct. 2024;31(1):218-29. https://doi.org/10.1080/15376494.2023.2231443

[14] Su M, Liu L, Xie Y, Peng H, Kang C. Prediction of the elastic properties and strength of unidirectional carbon fiber reinforced polymers based on representative volume element simulation. Case Stud Constr Mater. 2025;23:e04963. https://doi.org/10.1016/j.cscm.2025.e04963

[15] Bai W, Gong Z, Li Y, Liu J. Determination of the representative volume element model critical size for carbon fiber reinforced polymer composites. Compos Sci Technol. 2023;234:109946. https://doi.org/10.1016/j.compscitech.2023.109946

[16] Faghidian SA. On non-linear flexure of beams based on non-local elasticity theory. Int J Eng Sci. 2018;124:49-63. https://doi.org/10.1016/j.ijengsci.2017.12.002

[17] Challamel N, Wang CM, Reddy JN, Faghidian SA. Equivalence between micromorphic, nonlocal gradient, and two-phase nonlocal beam theories. Acta Mech. 2025;236(2):871-902. https://doi.org/10.1007/s00707-024-04180-x

[18] Hassanzadeh-Aghdam MK, Mahmoodi MJ, Ansari R. Micromechanical characterizing the effective elastic properties of general randomly distributed CNT-reinforced polymer nanocomposites. Probab Eng Mech. 2018;53:39-51. https://doi.org/10.1016/j.probengmech.2018.05.004

[19] Kassa MK, Arumugam AB. Micromechanical modeling and characterization of elastic behavior of carbon nanotube-reinforced polymer nanocomposites: A combined numerical approach and experimental verification. Polym Compos. 2020;41(8):3322-39. https://doi.org/10.1002/pc.25622

[20] Zaccardi F, Santonicola MG, Laurenzi S. Role of interface bonding on the elastic properties of epoxy-based nanocomposites with carbon nanotubes using multiscale analysis. Compos Struct. 2021;255:113050. https://doi.org/10.1016/j.compstruct.2020.113050

[21] Chwał M, Muc A. FEM micromechanical modeling of nanocomposites with carbon nanotubes. Rev Adv Mater Sci. 2021;60:342-51. https://doi.org/10.1515/rams-2021-0027

[22] Omari MA, Gharaibeh DT, Al-Momani ES. A comprehensive study of carbon nanoparticle shape and orientation effects on composite elastic properties using FEA. Mater Res Express. 2024;11(7):075005. https://doi.org/10.1088/2053-1591/ad5f0c

[23] Yengejeh SI, Kazemi SA, Öchsner A. Carbon nanotubes as reinforcement in composites: A review of the analytical, numerical and experimental approaches. Comput Mater Sci. 2017;136:85-101. https://doi.org/10.1016/j.commatsci.2017.04.023

[24] Moradi A, Ansari R, Hassanzadeh-Aghdam MK, Jamali J. Evaluating the role of agglomerated carbon nanotubes in the effective properties of polymer nanocomposites: An efficient micromechanics-based finite element framework. Comput Mater Sci. 2025;246:113337. https://doi.org/10.1016/j.commatsci.2024.113337

[25] CEA. Developing in Cast3M: User and developer documentation. Commissariat à l'Énergie Atomique et aux Énergies Alternatives (CEA); 2023. Available from: https://www-cast3m.cea.fr

[26] CEA. Optimization in Cast3M. Commissariat à l'Énergie Atomique et aux Énergies Alternatives (CEA); 2023. Available from: https://www-cast3m.cea.fr/html/charras/Optimisation_dans_Cast3M.pdf

[27] Efendy MGA, Pickering KL. Comparison of strength and Young modulus of aligned discontinuous fibre PLA composites obtained experimentally and from theoretical prediction models. Compos Struct. 2019;208:566-73. https://doi.org/10.1016/j.compstruct.2018.10.057

[28] Kareem S, Al-Ansari LS, Gömze LA. Modeling of modulus of elasticity of nano-composite materials: review and evaluation. J Phys Conf Ser. 2022;2315(1):012038. https://doi.org/10.1088/1742-6596/2315/1/012038

[29] Horio M, Onogi S. Dynamic measurements of physical properties of pulp and paper by audiofrequency sound. J Appl Phys. 1951;22(7):971-7. https://doi.org/10.1063/1.1700081

[30] Balan B, Reddy B, Narayana KB. Development of a code to generate randomly distributed short-fiber composites to estimate mechanical properties using FEM. Int J Theor Appl Mech. 2017;12(4):863-72.

[31] Daniel IM, Ishai O. Engineering mechanics of composite materials. 2nd ed. New York: Oxford University Press; 2006.

[32] Cox HL. The elasticity and strength of paper and other fibrous materials. Br J Appl Phys. 1952;3(3):72-9. https://doi.org/10.1088/0508-3443/3/3/302

[33] Sotomayor OE, Pancho A. Comparison of micromechanical models for predicting the Young's modulus of fiber-reinforced epoxy. Rev Politec. 2024;54(2):47-55. https://doi.org/10.33333/rp.vol54n2.04

[34] Jasti A, Chandra BA, Biswas S. Modified Halpin–Tsai model for predicting the mechanical properties of polymer composites reinforced with different cross-sectional fibers. Mater Today Proc. 2023;91:14-8. https://doi.org/10.1016/j.matpr.2023.04.131

[35] Xu Z, Shao X, Huang Q. A micromechanical model of multi-scale nano-reinforced composites. Polym Test. 2023;125:108121. https://doi.org/10.1016/j.polymertesting.2023.108121

[36] Zhou Y, Li J, Chirukam BN, Zhang Y, Lu C. A micromechanical modeling approach for predicting the piezoelectric and mechanical properties of piezoelectric fiber-reinforced multiphase composites containing CNT/GNP hybrids. J Intell Mater Syst Struct. 2024;35(4):424-39. https://doi.org/10.1177/1045389X231220206

[37] Nguyen DT, Manh ND, Dzung NM, Ninh DG. Highly efficient prediction of beating phenomena in laminated nanocomposite plates using a hybrid neural–numerical–analytical framework. Eur J Mech A Solids. 2026;116:105844. https://doi.org/10.1016/j.euromechsol.2025.105844

[38] Pan N. The elastic constants of randomly oriented fiber composites: A new approach to prediction. Sci Eng Compos Mater. 1996;5(2):63-72. https://doi.org/10.1515/SECM.1996.5.2.63

[39] Piggott MR. Load bearing fiber composites. Oxford: Pergamon Press; 1980. https://doi.org/10.1016/C2013-0-05885-9

[40] Lee DJ. On studies of tensile properties in injection molded short carbon fiber reinforced PEEK composite. KSME J. 1996;10(3):362-71. https://doi.org/10.1007/BF02942645

[41] Zhang X, Li W, Yang M, Zhao Z, He Y, Zheng S, et al. Temperature-dependent tensile strength of CNT/polymer nanocomposites considering the effects of CNT networks and waviness: Characterization and modeling. Polymer. 2022;263:125526. https://doi.org/10.1016/j.polymer.2022.125526

[42] Su X, Wang R, Li X, Araby S, Kuan HC, Naeem M, et al. A comparative study of polymer nanocomposites containing multi-walled carbon nanotubes and graphene nanoplatelets. Nano Mater Sci. 2022;4(3):185-204. https://doi.org/10.1016/j.nanoms.2021.08.003

[43] Takakura A, Beppu K, Nishihara T, Fukui A, Kozeki T, Namazu T, et al. Strength of carbon nanotubes depends on their chemical structures. Nat Commun. 2019;10(1):3040. https://doi.org/10.1038/s41467-019-10959-7

[44] Tahouneh V, Mashhadi MM, Naei MH. Finite element and micromechanical modeling for investigating effective material properties of polymer–matrix nanocomposites with microfiber reinforced by CNT arrays. Int J Adv Struct Eng. 2016;8(3):297-306. https://doi.org/10.1007/s40091-016-0132-y

[45] Moheimani R, Hasansade M. A closed-form model for estimating the effective thermal conductivities of carbon nanotube–polymer nanocomposites. Proc Inst Mech Eng C J Mech Eng Sci. 2019;233(8):2909-19. https://doi.org/10.1177/0954406218797967

[46] Kim HS, Jang J, Yu J, Kim SY. Thermal conductivity of polymer composites based on the length of multi-walled carbon nanotubes. Compos Part B Eng. 2015;79:505-12. https://doi.org/10.1016/j.compositesb.2015.05.012

[47] Yuan J, Yu S, Wang Y, Chen X, Zhou S, Zhong J, et al. Nanocarbon-enhanced cement composites for self-sensing and monitoring in transport infrastructure. Case Stud Constr Mater. 2024;21:e04082. https://doi.org/10.1016/j.cscm.2024.e04082

[48] Brek S, Meddour B, Groun B. Numerical modeling of the effects of fiber packing and reinforcement volume ratio on the transverse elasticity modulus of a unidirectional composite material glass/epoxy. Rev Compos Mater Av. 2020;30(5-6):203-10. https://doi.org/10.18280/rcma.305-602

[49] The French Alternative Energies and Atomic Energy Commission (CEA). Meshing: Cast3M documentation. CEA; 2023. Available from: https://www-cast3m.cea.fr

[50] Shirode Y, Thorat S, Jangle A, Ugale O, Kakad A, Shaikh MRN. An overview of carbon nanotubes and their approaches. J Pharm Biol Sci. 2024;12(2):119-26. https://doi.org/10.18231/j.jpbs.2024.018

[51] Power A, Gorey B, Chandra S, Chapman J. Carbon nanomaterials and their application to electrochemical sensors: A review. Nanotechnol Rev. 2018;7(1):19-41. https://doi.org/10.1515/ntrev-2017-0160

[52] Arora G, Pathak H. Modeling of transversely isotropic properties of CNT-polymer composites using meso-scale FEM approach. Compos Part B Eng. 2019;166:588-97. https://doi.org/10.1016/j.compositesb.2019.02.061

[53] Greco A. FEM analysis of the elastic behavior of composites and nanocomposites with arbitrarily oriented reinforcements. Compos Struct. 2020;241:112095. https://doi.org/10.1016/j.compstruct.2020.112095